The Disproportionate Role of Ocean Topography on the Upwelling of Carbon in the Southern Ocean

Riley Xavier Brady[1], Mathew E Maltrud[2], Phillip Justin Wolfram Jr.[3], Henri Francois Drake[4], and Nicole Suzanne Lovenduski[1]

[1]University of Colorado Boulder
[2]Los Alamos National Laboratory (DOE)
[3]Los Alamos National Laboratory
[4]Massachusetts Institute of Technology

November 28, 2022

Abstract

The physical circulation of the Southern Ocean sets the surface concentration and thus air-sea exchange of CO2. However, we have a limited understanding of the three-dimensional circulation that brings deep carbon-rich waters to the surface. Here, we introduce and analyze a novel high-resolution ocean model simulation with active biogeochemistry and online Lagrangian particle tracking. We focus our attention on a subset of particles with high dissolved inorganic carbon (DIC) that originate below 1000 m and eventually upwell into the surface mixed layer. We find that 71% of the DIC-enriched water upwelling across 1000 m is concentrated near topographic features, which occupy just 33% of the Antarctic Circumpolar Current. Once particles upwell to the surface mixed layer, their DIC decorrelates on timescales of ˜1.5 months—an order of magnitude longer than their residence time. Our results show that Southern Ocean bathymetry plays a key role in delivering carbon-rich waters to the surface.

The Disproportionate Role of Ocean Topography on the Upwelling of Carbon in the Southern Ocean

Riley X. Brady[1], Mathew E. Maltrud[2], Phillip J. Wolfram[2], Henri F. Drake[3], and Nicole S. Lovenduski[1]

[1]Department of Atmospheric and Oceanic Sciences and Institute of Arctic and Alpine Research, University of Colorado, Boulder, CO, USA
[2]Fluid Dynamics and Solid Mechanics (T-3), Los Alamos National Laboratory, Los Alamos, NM, USA
[3]MIT-WHOI Joint Program in Oceanography/Applied Ocean Science & Engineering, Cambridge and Woods Hole, MA, USA.

Key Points:

- We simulate the biogeochemical properties of online Lagrangian particles in the Southern Ocean
- Ocean bathymetry plays a disproportionate role in bringing deep, carbon-rich water to the Southern Ocean surface
- Once topographically influenced particles upwell to the surface, their carbon is transformed at the same rate as other mixed layer particles

Corresponding author: Riley X. Brady, `riley.brady@colorado.edu`

Abstract

The physical circulation of the Southern Ocean sets the surface concentration and thus air-sea exchange of CO_2. However, we have a limited understanding of the three-dimensional circulation that brings deep carbon-rich waters to the surface. Here, we introduce and analyze a novel high-resolution ocean model simulation with active biogeochemistry and online Lagrangian particle tracking. We focus our attention on a subset of particles with high dissolved inorganic carbon (DIC) that originate below 1000 m and eventually upwell into the surface mixed layer. We find that 71% of the DIC-enriched water upwelling across 1000 m is concentrated near topographic features, which occupy just 33% of the Antarctic Circumpolar Current. Once particles upwell to the surface mixed layer, their DIC decorrelates on timescales of ∼1.5 months—an order of magnitude longer than their residence time. Our results show that Southern Ocean bathymetry plays a key role in delivering carbon-rich waters to the surface.

Plain Language Summary

The Southern Ocean is the only place in the world where ocean currents circle the globe without hitting land. Here, some of the strongest winds on the planet force water to flow west-to-east around Antarctica and bring water from kilometers deep up to the surface. These waters have traversed the deep ocean for centuries, and in that time have gathered large stores of carbon from dead algae that rain down from above. When this water is brought to the surface, it expels its large store of carbon to the atmosphere. This process is important for the carbon cycle, but has not been extensively studied. Here, we use a new ocean model simulation that estimates ocean carbon and follows virtual floats that flow around the ocean and measure simulated carbon levels. We use the model to figure out how deep carbon in the Southern Ocean reaches the surface. We find that a large fraction of the carbon that is brought up from depth to the surface occurs in a relatively small fraction of the Southern Ocean, near places with mountains on the sea floor. Our study demonstrates that mountains on the sea floor have an influence on the global carbon cycle.

1 Introduction

The physical circulation of the Southern Ocean is paramount to its carbon cycling (e.g., Lovenduski et al., 2008, 2013; Landschützer et al., 2015). The region is characterized by a meridional overturning circulation whose upwelling limb brings deep waters enriched in old, respired carbon (Mikaloff Fletcher et al., 2007) to the surface (e.g., Marshall & Speer, 2012; Morrison et al., 2015). Once this natural CO_2 is released to the atmosphere it modifies the global carbon cycle and climate system (Gruber et al., 2009).

Substantial progress has been made in studying the Southern Ocean carbon cycle along the air–sea interface (see Gruber et al. (2019)), albeit through the lens of limited observations. Due to the region's harsh conditions, the majority of observations have been biased to the austral summer and to areas with frequent ship traversals that resupply Antarctic research stations (Munro et al., 2015). Autonomous ocean profiling floats have recently been outfitted with sensors to estimate biogeochemical quantities, such as ocean pH, from which the partial pressure of CO_2 (pCO_2) and the air-sea CO_2 flux can be derived (Johnson et al., 2017). These floats have begun to fill the seasonal and spatial gaps in our record and suggest that there is much stronger outgassing of CO_2 occurring in the Southern Ocean than previously estimated (Gray et al., 2018; Bushinsky et al., 2019). The unaccounted-for outgassing is inferred from elevated surface ocean pCO_2 measurements in the upwelling limb of the Antarctic Circumpolar Current (ACC), between the Polar Frontal Zone and seasonal sea ice edge (Gray et al., 2018). Factors contributing to carbon transport from depth remain a mystery and further investigation requires an

analysis of the physical underpinnings that contribute to dissolved CO_2 concentrations in the Southern Ocean.

Previous studies using Lagrangian ocean simulations suggest that vigorous upwelling in the Southern Ocean is confined to a few key regions, rather than occurring in a broad-band fashion across all longitudes of the ACC (Sallée et al., 2010; Viglione & Thompson, 2016; Tamsitt et al., 2017). These upwelling hot spots tend to occur downstream of topographic features. Due to the conservation of potential vorticity, topographic features steer the ACC equatorward, causing jets in the ACC to converge (Rintoul, 2018). This convergence steepens isopycnals and promotes stronger eddy activity downstream of the bathymetry, intensifying the local residual upwelling (Rintoul, 2018; Youngs, 2020). While previous model-based Lagrangian studies illuminated zonal asymmetries in Southern Ocean upwelling (Sallée et al., 2010; Viglione & Thompson, 2016; Tamsitt et al., 2017), no Lagrangian study has assessed the impact of upwelling hot spots on biogeochemical tracers. Further, these studies were conducted with "offline" Lagrangian particles, where trajectories are calculated using time-averaged velocity output from an Eulerian simulation, which can introduce unrecoverable error relative to using instantaneous velocities from the model (Qin et al., 2014).

Here, we aim to build upon the findings of previous Lagrangian studies of upwelling in the Southern Ocean by introducing and analyzing a novel global high-resolution ocean model simulation with active biogeochemistry and *online* Lagrangian particle tracking (i.e., at model runtime) for reduced error. Our Lagrangian particles are outfitted with virtual "sensors" that record the time history of physical and biogeochemical tracers along their trajectories, which allows us to consider the upwelling of dissolved CO_2. We view this problem from a three-dimensional perspective that follows transport pathways, aiming to better understand the deep origins of high-pCO_2 waters, the locations in which they upwell, and their potential for air-sea CO_2 exchange once they reach the mixed layer. Here, topographic contributions to Southern Ocean CO_2 outgassing are evaluated using Lagrangian analysis to understand the ocean transport of CO_2, a key driver of the global carbon cycle.

2 Methods

2.1 Model Configuration

Our primary modeling tool is the ocean and sea ice components of the Energy Exascale Earth System Model (E3SM; Golaz et al. (2019); Burrows et al. (2020)), the Model for Prediction Across Scales Ocean (MPAS-O) and the Model for Prediction Across Scales Sea Ice (Ringler et al., 2013). Our simulation is forced by momentum, heat, and freshwater fluxes from the Coordinated Oceanice Reference Experiments II (COREII) interannual atmospheric forcing dataset (Large & Yeager, 2009). The ocean model component also includes active biogeochemistry, which is based on the Biogeochemical Elemental Cycling (BEC) model (Moore et al., 2013).

We use an unstructured hexagonal mesh (Figure S1) with a horizontal resolution varying from 30 km at the equator to 10 km at the poles (Figure S2). In the latitude range of the ACC (50^oS - 60^oS), the horizontal resolution is an eddy-permitting 14.5 km (Figure S2). The model has 80 vertical levels with a vertical resolution varying from 2 m at the surface to 150 m at depth and uses a z-star coordinate system (Petersen et al., 2015).

The atmospheric CO_2 boundary condition in our simulation is a constant 360 ppm, chosen to align with the main collection period for biogeochemical observations used to initialize the simulation (Key et al., 2004). While this atmospheric CO_2 concentration is well above pre-industrial levels of $\sim$270 ppm, we focus on the circulation of deep, natural (pre-industrial) carbon to the surface, rather than the small surface perturbation due to anthropogenic carbon.

See the supporting information for more details on model parameterizations, the ocean biogeochemical model, and model initialization and spinup (Text S1).

2.2 Lagrangian Particle Tracking System

Following the model spinup, we seeded the global ocean with approximately one million Lagrangian particles using Lagrangian, in Situ, Global, High-Performance Particle Tracking (LIGHT), which was written specifically for MPAS-O (Wolfram et al., 2015). Particles were seeded at cell centers, with 15 particles linearly spread over the ocean depth of the given grid cell. Cell seeding locations were then horizontally downsampled using algebraic multi-grid splitting from PyAMG (Olson & Schroder, 2018). This resulted in approximately 300,000 particles initialized south of 45°S, which induced effectively no additional computational cost to the simulation (Wolfram et al., 2015).

The governing equation used for particle advection is

$$\frac{d\mathbf{x}}{dt} = \mathbf{u}\left[\mathbf{x}(t),\ t\right], \tag{1}$$

where three-dimensional Eulerian velocities from MPAS-O ($\mathbf{u}$) were interpolated to particle positions ($\mathbf{x}$) using Wachspress interpolation (Gillette et al., 2012). Particle trajectories were integrated at model runtime using second-order Runge-Kutta with two-hourly averages of the velocity fields, composed of the ten-minute model time steps.

Note that we only advect particles with velocities resolved by the model. In other words, we do not use any stochastic terms for subgrid-scale processes such as mixing and diffusion, consistent with other model Lagrangian particle studies (e.g., Tamsitt et al., 2017; Drake et al., 2018). This approach is justified in our study, as upwelling throughout the interior of the ACC is generally adiabatic (Marshall & Speer, 2012), and most of our analysis focuses on particle behavior prior to reaching the mixed layer.

We simulated LIGHT particles for 17 years, which matches the 17-year mode of the transit time distribution for Circumpolar Deep Water to reach the Southern Ocean surface at this model resolution (Drake et al., 2018). Trajectories were saved to disk every two days, recording instantaneous x, y, and z positions as well as instantaneous temperature, salinity, dissolved inorganic carbon (DIC), alkalinity, PO_4, NO_3, and SiO_3. Tracers were similarly interpolated from cell centers to particle positions using Wachspress interpolation (Gillette et al., 2012). Quantities such as pCO_2 and potential density (σ_0) were then calculated diagnostically using the recorded tracer values. See Movie S1 for a demonstration of the Lagrangian advection of DIC at depth over the course of one model year.

2.3 Model Evaluation

Comprehensive validation of a CORE-II-forced MPAS-O simulation can be found in Petersen et al. (2019). They show that MPAS-O does a suitable job at replicating ocean currents, heat transport, sea ice coverage, sea surface temperature, and salinity. The high-resolution mesh used in this study is capable of replicating strongly eddying flows, such as the ACC (Petersen et al., 2019). We provide further evaluation of our MPAS-O simulation in the supporting information, focusing on horizontal transport of the ACC, mixed layer depth, and deep concentrations of DIC. In summary, our model finds general agreement in all three fields against observations, with relatively high pattern correlations and relatively low error within the ACC (Figures S3-S5).

3 History of an Upwelled Particle

We begin by introducing the reader to an example particle trajectory (Figure 1); this narrative puts the methodology section into practice and helps to frame the forthcoming results, which will divide particles into groups for ensemble analysis. The particular particle on which we focus is initialized just beneath 1000 m in the central Pacific sector of the ACC (Figure 1a). Its final deep upwelling across 1000 m occurs just under two years into its transit, coinciding with shallow bathymetry in the Drake Passage (Figure 1a). Note that we emphasize the *final* upwelling across 1000 m to avoid statistical artifacts from particles that oscillate at high frequency around 1000 m. The particle then circumnavigates the ACC with nearly monotonic upwelling, first crossing into 200 m near the Campbell Plateau (Figure 1). Upon entering the Drake Passage for a second time—around 15.5 years into its trajectory—the particle abruptly downwells and oscillates around a depth of approximately 350 m, ending its voyage in the Patagonian Shelf (Figure 1).

We identify the statistical origin of DIC using its e-folding decorrelation time scale—or "memory time" (Cetina-Heredia et al., 2018)—over the time series segment prior to upwelling across 1000 m and between the 1000 m and 200 m crossings. The memory time analysis is used to make an unbiased estimate of the source of DIC for a given particle, rather than to diagnose the processes leading to the decorrelation of the tracer. We identify the location of the DIC source for the upwelled particle by backward estimates of its corresponding memory time; the statistical source of DIC on this particular particle is indicated with red (1000 m) and pink (200 m) dots on Figure 1b. The DIC memory time of the particle prior to upwelling across 1000 m is about two months. This corresponds to a DIC source approximately 650 km upstream of the Drake Passage. On the other hand, the DIC memory time over its 1000 m to 200 m transit is roughly 5.5 years, corresponding to an upstream DIC source that has traversed nearly half the distance of the ACC—or 10,500 km (Figure 1b).

Prior to upwelling into the mixed layer, our example particle stores large amounts of carbon, averaging a DIC concentration of $\sim$2220 μmol kg^{-1} and a potential pCO_2 of $\sim$560 μatm. This potential pCO_2 is 200 μatm higher than the atmosphere, which would lead to rapid outgassing of CO_2 from the ocean. Potential pCO_2 represents the pCO_2 that the particle would have upon reaching 200 m, based on the ambient temperature of the mixed layer where and when the particle upwells, provided that there are no changes to DIC due to biology or circulation (Sarmiento & Gruber, 2006). Upon upwelling to 400 m depth just past the Kerguelan Plateau, the particle rapidly loses its carbon. Over the course of four months, the particle stays between 400 m and 250 m depth and loses 50 μmol kg^{-1} of DIC and 90 μatm of potential pCO_2. The particle then upwells past 200 m and stays above this depth for nearly two years while traversing the Pacific Ocean between the Campbell Plateau and Drake Passage (Figure 1b). Here, surface processes such as photosynthesis and air-sea heat and gas exchange likely reduce the particle's potential pCO_2 enough for it to uptake CO_2 from the atmosphere during the austral summer and fall (December through April). Upon reaching the Drake Passage, the particle subducts between depths of 200 m and 500 m.

The example particle trajectory outlined in this section demonstrates how we can apply statistical methods to our tracer time series to better understand the behavior of upwelled carbon in the Southern Ocean. We now turn to an ensemble view of particle trajectories to glean understanding of the bulk behavior of carbon upwelled in the Southern Ocean.

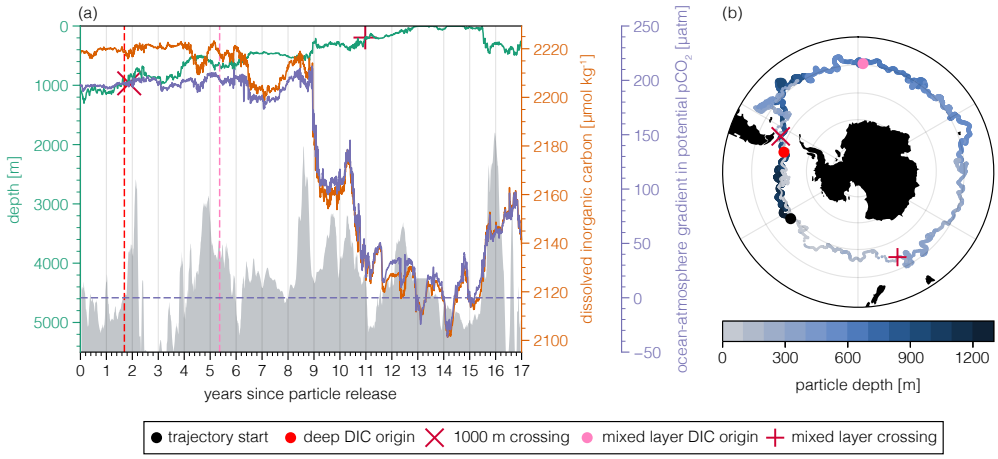

Figure 1. Tracer and location history of an upwelled particle in the Southern Ocean. (a) Depth (green), dissolved inorganic carbon (DIC; orange), and the potential pCO_2 gradient between the ocean and atmosphere (purple) over the 17-year particle history. The gray shading shows the ocean bathymetry from the nearest Eulerian grid cell and is smoothed over a 15-day centered rolling average. Potential pCO_2 represents the pCO_2 the particle would have if it were brought to 200 m without any circulation- or biology-driven changes and warmed or cooled to the ambient temperature at the location and time in which it crossed into 200 m (Sarmiento & Gruber, 2006). Potential pCO_2 is subtracted by the fixed atmospheric CO_2 concentration of 360 μatm. Thus, when potential pCO_2 is positive (above the purple dashed line), it would outgas carbon to the atmosphere. When negative (below the purple dashed line), it would uptake CO_2 from the atmosphere. (b) Spatial history of the Lagrangian trajectory. The particle starts at the black dot in the Pacific sector and circumnavigates the Antarctic Circumpolar Current, ending near the Patagonian Shelf off of South America. The color of the trajectory denotes the particle depth and the thickness of the line is proportional to the concentration of DIC. The red "X" (in panels a and b) shows the first 1000 m crossing of the particle and the red circle (red dashed line in panel a) shows the statistical source of DIC for the 1000 m crossing. The pink "+" shows the subsequent 200 m crossing of the particle and the pink circle (pink dashed line in panel a) shows the statistical source of DIC for the 200 m crossing. This source was computed using the *e*-folding decorrelation time scale (or "memory time") of DIC prior to 1000 m and between 1000 m and 200 m following Cetina-Heredia et al. (2018).

4 Ensemble Analysis of Upwelled Carbon

Topographic features have a disproportionate influence on the upwelling of particles across both 1000 m and 200 m in our simulation (Figure 2). Following Tamsitt et al. (2017), we organize particle trajectories into ensembles based on the location in which they last upwell across 1000 m in the Southern Ocean. We ignore particles that upwell within the model's 75% annual sea ice extent to keep focus on upwelling occurring within the ACC. We further subset this by particles that ultimately reach at least 200 m before the simulation ends, to focus on particles that have an influence on mixed layer properties. This results in a sample of 19,002 particles (Table 1).

We identify four topographic regions that represent just 33% of the surface area of the ACC, but contribute to 71% of the total deep particle upwelling: the Drake Pas-

sage, Crozet Plateau, Kerguelan Plateau, and Campbell Plateau (Figure 2a; Table 1). These four regions are similar to those outlined in previous studies that identify the outsized influence of topography on Southern Ocean upwelling (Sallée et al., 2010; Viglione & Thompson, 2016; Tamsitt et al., 2017). Roughly 65% of particles that upwell across 1000 m within the ACC first reach 200 m within the ACC as well (Figure 2b). Of the remaining particles, 32% upwell into 200 m beneath the sea ice and 3% upwell into the mixed layer north of 45°S. Note that we analyze the location in which particles *first* cross into the mixed layer (after their *last* 1000 m crossing), to assess where they initially influence and communicate with the upper ocean and atmosphere. Although upwelling across 200 m is seemingly more spatially diffuse than across 1000 m, our four regions that represent 33% of the surface area of the ACC contribute to 63% of the total mixed layer particle upwelling (Figure 2a; Table 1). Thus, ocean topography has a disproportionate influence on upwelling of water both in deep (at 1000 m) and shallow (at 200 m) waters.

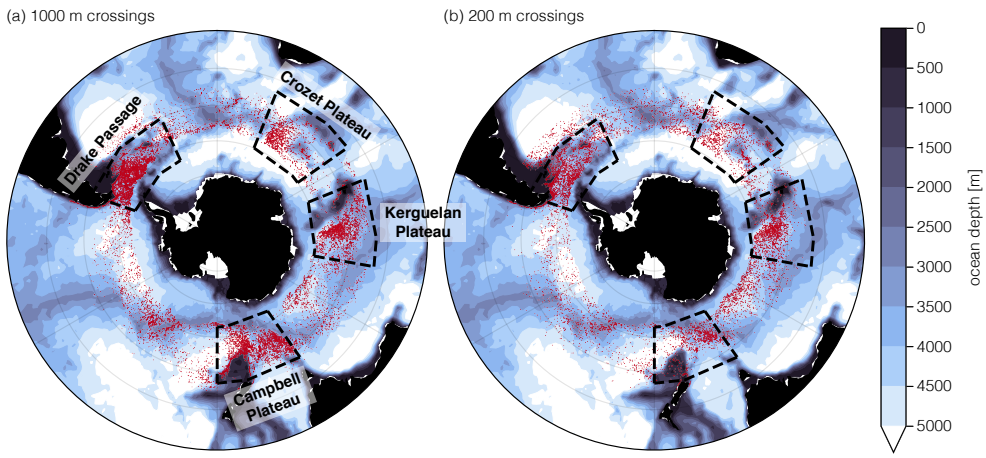

Figure 2. Upwelling locations of Lagrangian particles in the Antarctic Circumpolar Current (ACC). (a) 1000 m upwelling locations that occurred in the ACC, south of 45°S and outside of the 75% annual sea ice zone. Only the *final* 1000 m particle crossings during their 17-year trajectories are shown, and particles that do not ultimately reach 200 m are not included (N = 19,002). Black dashed boxes show the four regions that are used for ensemble analysis, which are associated with topographic features and a disproportionate amount of upwelling relative to the region's surface area: the Drake Passage, Campbell Plateau, Kerguelan Plateau, and Crozet Plateau. (b) 200 m upwelling locations. Crossings are only shown for the particles from (a) whose first 200 m upwelling (following the 1000 m crossing) occurred south of 45°S and outside of the 75% annual sea ice zone (N = 12,301). Ocean bathymetry from the Eulerian model mesh is shown in purple contours.

Deep upwelled carbon is generally sourced from waters upstream of topographic features in a relatively narrow meridional band (Figure 3). Source waters of deep carbon span approximately 800 km – 1000 km meridionally, drawing primarily from the ACC region (Figure 3; Table 1). However, a notable exception is the Kerguelan Plateau region, which draws DIC from subtropical waters originating in the Agulhas Return Current over 1000 km away (Figure 3c). DIC source waters for deep upwelling vary much more zonally than meridionally between topographic regions (Table 1). The Campbell Plateau draws DIC from waters spanning a zonal range of 4,900 km—nearly one-quarter of the ACC (Figure 3d; Table 1). On the other hand, the Kerguelan Plateau DIC source

originates from a much more narrow zonal band of 3,700 km (Figure 3c; Table 1). The Crozet Plateau and Drake Passage regions bring deep carbon from a zonal extent of 4,100 to 4,700 km (Figure 3a and b; Table 1).

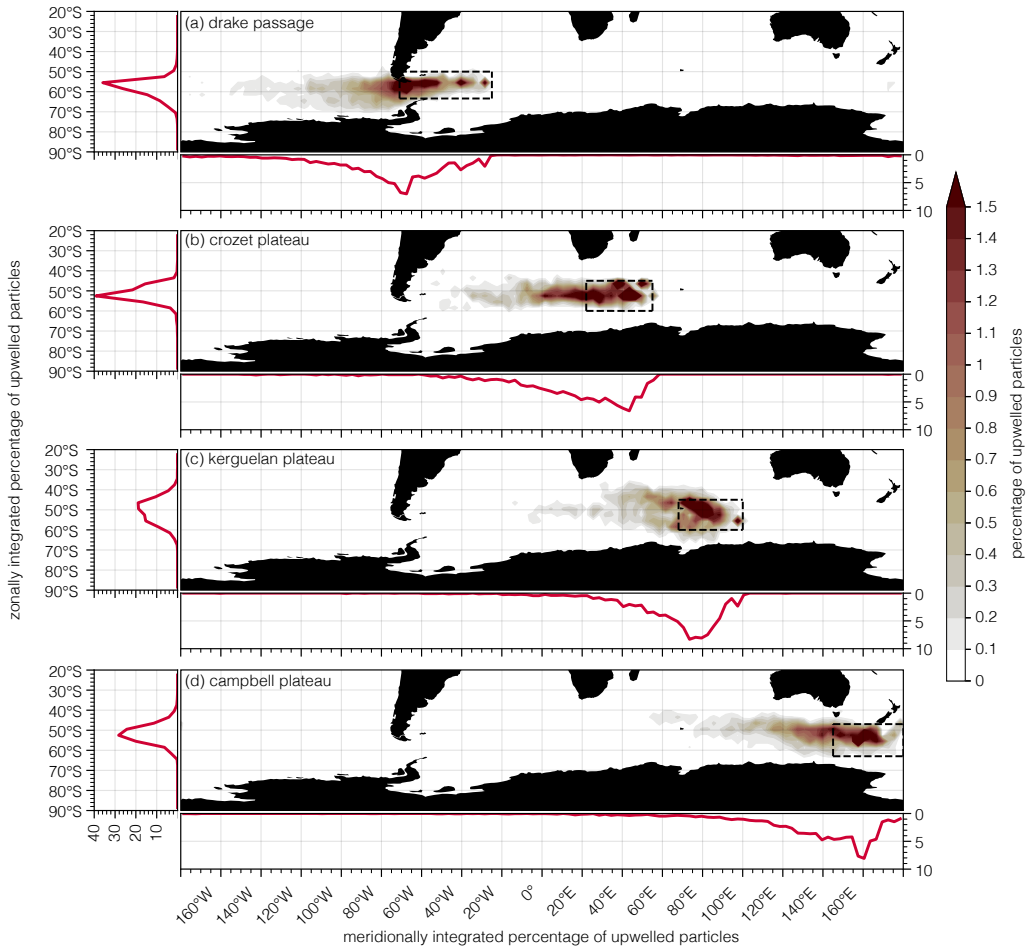

Figure 3. Statistical origin of deep (1000 m upwelled) dissolved inorganic carbon (DIC) for the four topographic regions. Particle ensembles were selected based on their final 1000 m upwelling location (see Figure 2) and were subset based on the dashed boxes in a-d. The maps in each panel show the memory time origin for each particle in the ensemble following Cetina-Heredia et al. (2018), based on the *e*-folding decorrelation time scale of the particle prior to its 1000 m upwelling. The memory time (M) is derived for each trajectory individually, and then the x-y coordinates are evaluated M time steps prior to the 1000 m crossing. The side panels associated with each subplot show the zonal (left) and meridional (bottom) sum for each panel. All values are reported as the percentage of all particles in the given ensemble.

Circumpolar Deep Water (CDW) is the dominant source of DIC upwelling across 1000 m in the topographically influenced regions (Figure 4a). However, Antarctic Intermediate Water (AAIW) also supplies a sizable portion of upwelled DIC in each of the regions. The Drake Passage (64%), Kerguelan Plateau (72.5%), and Crozet Plateau (86%) source a majority of their DIC from CDW, with the remainder attributed to the lighter AAIW (Figure 4a). The Campbell Plateau is a unique region, in that its sourced DIC

is roughly split between CDW (46%) and AAIW (47.5%), with the remainder attributed to Subantarctic Mode Water (SAMW; Figure 4a). Despite the differences in water mass characteristics of source waters, all four regions upwell waters that are enriched with high concentrations of DIC and a large store of potential pCO_2 relative to the atmosphere (Figures 4b and c; Table 1). Source water DIC varies in a narrow range of 2,212 to 2,220 μmol kg^{-1} (Table 1). These carbon stores translate to waters with a strong outgassing potential. All four regions have a median potential pCO_2 ranging from 130 to 150 μatm higher than the fixed atmospheric concentration of 360μatm, and 99.9% of all source waters tend toward outgassing potential rather than uptake potential (Figure 4c; Table 1).

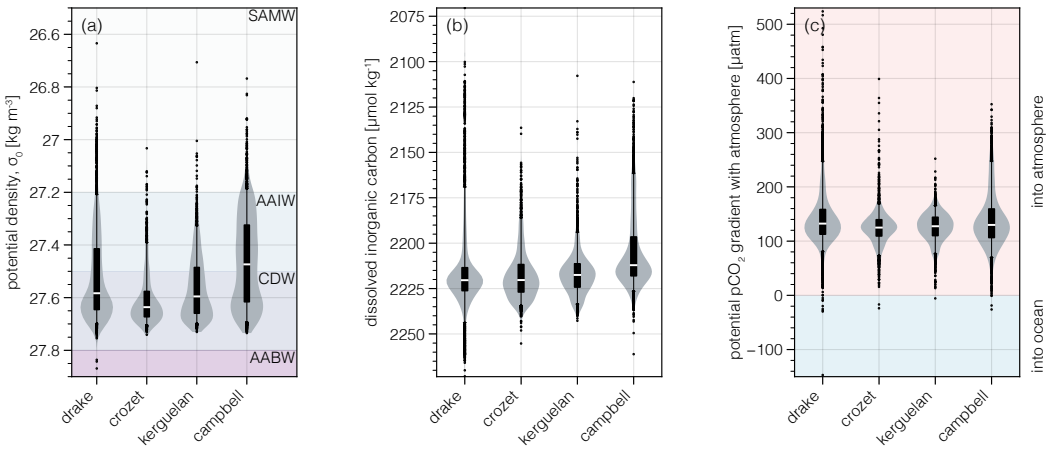

Figure 4. Properties of deep (1000 m) upwelled waters in the Southern Ocean. Properties are based on the memory time (*e*-folding decorrelation time scale; Cetina-Heredia et al. (2018)) for dissolved inorganic carbon (DIC) prior to upwelling across 1000 m in the given topographic region. The memory time (M) is derived for each trajectory individually, and then tracer concentrations are evaluated M time steps prior to the 1000 m crossing. Boxes outline the 25% and 75% quantiles, with the white line showing the median. Whiskers outline the 5% and 95% quantiles, with black dots showing outliers (the remaining 10% of the data). The grey violin plots show the underlying distribution of the tracers. (a) DIC, (b) potential density (referenced to the surface), and (c) potential pCO_2 minus the fixed atmospheric concentration of 360 μatm. Potential pCO_2 represents what the pCO_2 concentration would be solely due to the thermal effects of bringing the particle from its current temperature to the ambient temperature when the given particle first upwells into 200 m (Sarmiento & Gruber, 2006). Water mass definitions are based on Schmitz (1996).

Upon reaching the mixed layer, the DIC transformation on the particles is generally similar, regardless of the deep upwelling pathway taken by the particle. On average, all particles entering the mixed layer have a DIC decorrelation time scale of 1.5 months (Table 1). The average residence time in the mixed layer is approximately one week (Table 1), suggesting that DIC does not fully equilibrate with the atmosphere during the average single stay in the mixed layer.

5 Conclusions & Discussion

We generated and analyzed a novel high-resolution simulation of a global ocean model with biogeochemistry and online Lagrangian particle tracking to illuminate the pathways

over which natural carbon upwells from depth in the Southern Ocean. Our particles were equipped with virtual "sensors" to record physical and biogeochemical properties along their trajectories. We found that ocean topography plays a key role in bringing carbon-enriched waters to the surface; we identified four regions with prominent topographic features that cover just one-third of the ACC, but are responsible for 71% of particle upwelling across 1000 m (Figure 2a; Table 1). All deep waters are enriched in DIC and have a high potential pCO_2 relative to the atmosphere (Figure 4b and c; Table 1). Topographic regions create zonal asymmetries in the meridional overturning of the Southern Ocean and act as a conduit for circulating this relatively uniform deep carbon supply to the surface. After reaching the mixed layer, the DIC behavior of upwelled particles are indistinguishable from one another, regardless of the particle's origin (Table 1). Our Lagrangian model analysis thus demonstrates that topographic features in the Southern Ocean bring disproportionately large quantities of the relatively uniform deep carbon stores to the surface, consistent with previous Eulerian analyses (Dufour et al., 2015). Further, our results indicate that the mixed layer residence time of particles is an order of magnitude shorter than the decorrelation time scale of DIC at the surface (Table 1). Particles remain above 200 m for roughly one week on average, but it takes 1.5 months for DIC to decorrelate (Table 1).

While this study presents a novel perspective on the three-dimensional circulation of carbon in the Southern Ocean, there are some caveats worth noting. First, our Lagrangian particle trajectories are only influenced by resolved advection, i.e., we do not include any stochastic terms to simulate diffusion and unresolved physics (Van Sebille et al., 2018), and this could affect our estimates of mixed layer residence times. However, our mesh has a horizontal resolution of $\sim$14.5 km in the ACC (Figure S2) and thus resolves the influence of mesoscale eddies on trajectories. Further, upwelling in the Southern Ocean follows nearly adiabatic pathways prior to reaching the mixed layer (Marshall & Speer, 2012). Second, we rely upon the accuracy of a single physical and biogeochemical model (MPAS-O and BEC) for our Lagrangian particle tracking system, which is biased relative to real world dynamics and biogeochemistry. However, our model evaluation and previous studies demonstrate that MPAS-O is suitable for simulating the circulation and sub-surface DIC concentrations of the Southern Ocean (Figures S3-S5; Petersen et al. (2019)). Third, our particle trajectories span 17 years, so we do not resolve the long tail of the transit time distribution for deep upwelling to the Southern Ocean surface (Drake et al., 2018). However, we do permit the mode of the transit time distribution (17 years), so our analysis likely includes the most representative trajectories. Our study required the use of a high-resolution horizontal mesh so that we could resolve mesoscale eddies and thus investigate the influence of topographic features on upwelling, which act to modify the eddy-driven component of Southern Ocean overturning (Rintoul, 2018; Youngs, 2020). Prioritizing the higher resolution of the model incurred significant computational cost, which limited the temporal extent of our particle trajectories. The conclusions reached in this study would not have been possible with a low-resolution model or offline particle tracking methods. Finally, we did not explore particles that upwelled under sea ice. Sea ice caps surface waters from the atmosphere, and potentially reduces air-sea gas exchange (Gupta et al., 2020). Since the bulk of upwelling and air-sea gas exchange occurs in the core of the ACC, we focus our analysis there.

Our study builds upon work done by Viglione and Thompson (2016) and Tamsitt et al. (2017) by connecting the zonal asymmetries in physical circulation to the marine carbon cycle. To our knowledge, our study marks the first global high-resolution ocean biogeochemistry experiment with online Lagrangian particle tracking. Our results showcase the fine-grained analysis that can be performed with a Lagrangian perspective of ocean biogeochemistry by tracing out the pathways over which carbon circulates in the Southern Ocean. There exists a tremendous amount of untapped biogeochemical information for future Lagrangian biogeochemical studies to reveal. Future studies could, for example, focus on the behavior of carbon upwelled under sea ice. Further, an analysis

similar to this could be conducted in many other regions of the world oceans, where carbon and other biogeochemical tracer pathways are under intense study (e.g., the California Current; Rykaczewski & Dunne, 2010; Pozo Buil & Di Lorenzo, 2017). While the computational expense of a high-resolution global online Lagrangian study is high, the insights gleaned from such a simulation are invaluable. In this case, we have found that seamounts and ridges on the Southern Ocean seafloor ultimately dictate the three-dimensional movement of deep carbon to the ocean's surface and have the potential to influence air-sea CO_2 exchange.

Acknowledgments

The Lagrangian particle output used in this study and the code used to generate the main figures and table in the text can be found on Zenodo under DOI: 10.5281/zenodo.4281539. RXB was supported by the Department of Energy's Computational Science Graduate Fellowship (DE-FG02-97ER25308), and particularly benefited from the fellowship's summer practicum at Los Alamos National Lab. NSL and RXB were further supported by the National Science Foundation (NSF-PLR 1543457; NSF-OCE 1924636; NSF-OCE 1752724; NSF-OCE 1558225). MEM and PJW were supported as part of the Energy Exascale Earth System Model (E3SM) project, funded by the U.S. Department of Energy, Office of Science, Office of Biological and Environmental Research. This research used resources provided by the Los Alamos National Laboratory Institutional Computing Program, which is supported by the U.S. Department of Energy National Nuclear Security Administration under Contract No. 89233218CNA000001. The Climate, Ocean and Sea Ice Modeling (COSIM) team at LANL provided invaluable feedback and support during the project.

Table 1. Geographic information and statistics for deep (1000 m) and mixed layer (200 m) upwelled particles that occur within and outside of topographic regions in the Southern Ocean. All values including ± indicate the median value ± the standard deviation. Parentheses indicate the extent of -1σ to 1σ in km. The decorrelation timescale of DIC above 200 m was calculated by assessing the e-folding time scale (i.e., the time at which the autocorrelation drops below 1/e) of every instance a particle from the given ensemble upwelled into 200 m, and the autocorrelation was statistically significant with $p < 0.05$. We also excluded 200 m crossings that occurred north of 45°S, within the 75% annual ice present zone, or within an ocean depth shallower than 500 m (to avoid coastally trapped particles). The residence time was computed alongside this calculation, and times were retained even in cases the particle did not decorrelate below $\frac{1}{e}$ or when the decorrelation was not statistically significant.

	Drake Passage	Crozet Plateau	Kerguelan Plateau	Campbell Plateau	Non-Topographic
		Geographic Information			
geographic coordinates	71°W – 25°W 63.4^{o}S – 50°S	22°E – 55°E 60°S – 45°S	68°E – 100°E 60°S – 45°S	145°E – 180°E 63°S – 47°S	—
% of ACC surface area	7.4%	8.1%	8.1%	9.2%	67.2%
		Deep Upwelling (1000 m) Statistics			
number of particles	5,645	2,050	2,181	3,651	5,475
% of deep upwelled particles	29.7%	10.8%	11.5%	19.2%	28.8%
zonal origin[b]	73.6^{o}W ± 39.6^o (4,740 km)	23.0^{o}E ± 30.4^o (4,150 km)	71.4^{o}E ± 26.0^o (3,690 km)	142.8^{o}E ± 35.8^o (4,910 km)	—
meridional origin[b]	57.4^{o}S ± 4.3^o (950 km)	52.1^{o}S ± 3.6^o (800 km)	50.3^{o}S ± 5.8^o (1280 km)	51.9^{o}S ± 4.3^o (960 km)	—
median DIC memory time (days)	366	410	382	338	366
σ_θ of source waters [kg m^{-3}]	27.6 ± 0.2	27.6 ± 0.1	27.6 ± 0.1	27.5 ± 0.2	27.5 ± 0.2
DIC of source waters [μmol kg^{-1}]	2220 ± 23	2220 ± 15	2217 ± 13	2212 ± 21	2218 ± 21
potential pCO_2 of source waters[a] [μatm]	486 ± 51	479 ± 33	481 ± 27	484 ± 51	482 ± 44
		Mixed Layer (200 m) Statistics			
number of particles[a]	3,104	1,646	1,632	1,393	4,526
% of upwelled particles	25.2%	13.4%	13.3%	11.3%	36.8%
decorrelation timescale of DIC (days)	44	44	44	42	40
residence time (days)	6	6	8	8	8

[a] particle ensembles are based on the location of their 200 m crossing, not their 1000 m crossing (as in Figure 2b).
[b] values are rounded to the nearest 10.

References

Burrows, S., Maltrud, M., Yang, X., Zhu, Q., Jeffery, N., Shi, X., ... others (2020). The DOE E3SM v1. 1 biogeochemistry configuration: description and simulated ecosystem-climate responses to historical changes in forcing. *Journal of Advances in Modeling Earth Systems*, e2019MS001766.

Bushinsky, S. M., Landschützer, P., Rödenbeck, C., Gray, A. R., Baker, D., Mazloff, M. R., ... Sarmiento, J. L. (2019). Reassessing Southern Ocean air-sea CO2 flux estimates with the addition of biogeochemical float observations. *Global biogeochemical cycles*, *33*(11), 1370–1388.

Cetina-Heredia, P., van Sebille, E., Matear, R. J., & Roughan, M. (2018). Nitrate sources, supply, and phytoplankton growth in the Great Australian Bight: An Eulerian-Lagrangian modeling approach. *Journal of Geophysical Research: Oceans*, *123*(2), 759–772.

Drake, H. F., Morrison, A. K., Griffies, S. M., Sarmiento, J. L., Weijer, W., & Gray, A. R. (2018). Lagrangian timescales of Southern Ocean upwelling in a hierarchy of model resolutions. *Geophysical Research Letters*, *45*(2), 891–898.

Dufour, C. O., Griffies, S. M., de Souza, G. F., Frenger, I., Morrison, A. K., Palter, J. B., ... others (2015). Role of mesoscale eddies in cross-frontal transport of heat and biogeochemical tracers in the Southern Ocean. *Journal of Physical Oceanography*, *45*(12), 3057–3081.

Gillette, A., Rand, A., & Bajaj, C. (2012). Error estimates for generalized barycentric interpolation. *Advances in computational mathematics*, *37*(3), 417–439.

Golaz, J.-C., Caldwell, P. M., Van Roekel, L. P., Petersen, M. R., Tang, Q., Wolfe, J. D., ... others (2019). The DOE E3SM coupled model version 1: Overview and evaluation at standard resolution. *Journal of Advances in Modeling Earth Systems*, *11*(7), 2089–2129.

Gray, A. R., Johnson, K. S., Bushinsky, S. M., Riser, S. C., Russell, J. L., Talley, L. D., ... Sarmiento, J. L. (2018). Autonomous biogeochemical floats detect significant carbon dioxide outgassing in the high-latitude Southern Ocean. *Geophysical Research Letters*, *45*(17), 9049–9057.

Gruber, N., Gloor, M., Mikaloff Fletcher, S. E., Doney, S. C., Dutkiewicz, S., Follows, M. J., ... others (2009). Oceanic sources, sinks, and transport of atmospheric CO2. *Global biogeochemical cycles*, *23*(1).

Gruber, N., Landschützer, P., & Lovenduski, N. S. (2019). The variable Southern Ocean carbon sink. *Annual review of marine science*, *11*, 159–186.

Gupta, M., Follows, M. J., & Lauderdale, J. M. (2020). The effect of Antarctic sea ice on Southern Ocean carbon outgassing: Capping versus light attenuation. *Global Biogeochemical Cycles*, *34*(8), e2019GB006489.

Johnson, K. S., Plant, J. N., Coletti, L. J., Jannasch, H. W., Sakamoto, C. M., Riser, S. C., ... others (2017). Biogeochemical sensor performance in the SOCCOM profiling float array. *Journal of Geophysical Research: Oceans*, *122*(8), 6416–6436.

Key, R. M., Kozyr, A., Sabine, C. L., Lee, K., Wanninkhof, R., Bullister, J. L., ... Peng, T.-H. (2004). A global ocean carbon climatology: Results from Global Data Analysis Project (GLODAP). *Global biogeochemical cycles*, *18*(4).

Landschützer, P., Gruber, N., Haumann, F. A., Rödenbeck, C., Bakker, D. C., Van Heuven, S., ... others (2015). The reinvigoration of the Southern Ocean carbon sink. *Science*, *349*(6253), 1221–1224.

Large, W., & Yeager, S. (2009). The global climatology of an interannually varying air–sea flux data set. *Climate dynamics*, *33*(2-3), 341–364.

Lovenduski, N. S., Gruber, N., & Doney, S. C. (2008). Toward a mechanistic understanding of the decadal trends in the Southern Ocean carbon sink. *Global Biogeochemical Cycles*, *22*(3).

Lovenduski, N. S., Long, M. C., Gent, P. R., & Lindsay, K. (2013). Multi-decadal trends in the advection and mixing of natural carbon in the Southern Ocean.

Geophysical research letters, *40*(1), 139–142.

Marshall, J., & Speer, K. (2012). Closure of the meridional overturning circulation through Southern Ocean upwelling. *Nature Geoscience*, *5*(3), 171–180.

Mikaloff Fletcher, S., Gruber, N., Jacobson, A. R., Gloor, M., Doney, S., Dutkiewicz, S., ... others (2007). Inverse estimates of the oceanic sources and sinks of natural CO2 and the implied oceanic carbon transport. *Global Biogeochemical Cycles*, *21*(1).

Moore, J. K., Lindsay, K., Doney, S. C., Long, M. C., & Misumi, K. (2013). Marine ecosystem dynamics and biogeochemical cycling in the Community Earth System Model [CESM1 (BGC)]: Comparison of the 1990s with the 2090s under the RCP4.5 and RCP8.5 scenarios. *Journal of Climate*, *26*(23), 9291–9312.

Morrison, A. K., Frölicher, T. L., & Sarmiento, J. L. (2015). Upwelling in the Southern Ocean. *Physics Today*, *68*(1), 27.

Munro, D. R., Lovenduski, N. S., Takahashi, T., Stephens, B. B., Newberger, T., & Sweeney, C. (2015). Recent evidence for a strengthening CO2 sink in the Southern Ocean from carbonate system measurements in the Drake Passage (2002–2015). *Geophysical Research Letters*, *42*(18), 7623–7630.

Olson, L. N., & Schroder, J. B. (2018). *PyAMG: Algebraic multigrid solvers in Python v4.0.* Retrieved from `https://github.com/pyamg/pyamg` (Release 4.0)

Petersen, M. R., Asay-Davis, X. S., Berres, A. S., Chen, Q., Feige, N., Hoffman, M. J., ... others (2019). An evaluation of the ocean and sea ice climate of E3SM using MPAS and interannual CORE-II forcing. *Journal of Advances in Modeling Earth Systems*, *11*(5), 1438–1458.

Petersen, M. R., Jacobsen, D. W., Ringler, T. D., Hecht, M. W., & Maltrud, M. E. (2015). Evaluation of the arbitrary Lagrangian–Eulerian vertical coordinate method in the MPAS-Ocean model. *Ocean Modelling*, *86*, 93–113.

Pozo Buil, M., & Di Lorenzo, E. (2017). Decadal dynamics and predictability of oxygen and subsurface tracers in the California Current System. *Geophysical Research Letters*, *44*(9), 4204–4213.

Qin, X., van Sebille, E., & Gupta, A. S. (2014). Quantification of errors induced by temporal resolution on Lagrangian particles in an eddy-resolving model. *Ocean Modelling*, *76*, 20–30.

Ringler, T., Petersen, M., Higdon, R. L., Jacobsen, D., Jones, P. W., & Maltrud, M. (2013). A multi-resolution approach to global ocean modeling. *Ocean Modelling*, *69*, 211–232.

Rintoul, S. R. (2018). The global influence of localized dynamics in the Southern Ocean. *Nature*, *558*(7709), 209–218.

Rykaczewski, R. R., & Dunne, J. P. (2010). Enhanced nutrient supply to the California Current ecosystem with global warming and increased stratification in an Earth system model. *Geophysical Research Letters*, *37*(21).

Sallée, J.-B., Speer, K., Rintoul, S., & Wijffels, S. (2010). Southern Ocean thermocline ventilation. *Journal of Physical Oceanography*, *40*(3), 509–529.

Sarmiento, J. L., & Gruber, N. (2006). *Ocean biogeochemical dynamics.* Princeton University Press.

Schmitz, W. J. (1996). On the world ocean circulation. volume II: The Pacific and Indian oceans–a global update. *Tech. Rep. WHOI-96-08*, 241.

Tamsitt, V., Drake, H. F., Morrison, A. K., Talley, L. D., Dufour, C. O., Gray, A. R., ... others (2017). Spiraling pathways of global deep waters to the surface of the Southern Ocean. *Nature communications*, *8*(1), 1–10.

Van Sebille, E., Griffies, S. M., Abernathey, R., Adams, T. P., Berloff, P., Biastoch, A., ... others (2018). Lagrangian ocean analysis: Fundamentals and practices. *Ocean Modelling*, *121*, 49–75.

Viglione, G. A., & Thompson, A. F. (2016). Lagrangian pathways of upwelling in the Southern Ocean. *Journal of Geophysical Research: Oceans*, *121*(8), 6295–

6309.

Wolfram, P. J., Ringler, T. D., Maltrud, M. E., Jacobsen, D. W., & Petersen, M. R. (2015). Diagnosing isopycnal diffusivity in an eddying, idealized midlatitude ocean basin via Lagrangian, in situ, global, high-performance particle tracking (LIGHT). *Journal of Physical Oceanography*, *45*(8), 2114–2133.

Youngs, M. K. (2020). *Residual overturning circulation and its connection to Southern Ocean dynamics* (Unpublished doctoral dissertation). Massachusetts Institute of Technology and the Woods Hole Oceanographic Institution.

Supporting Information for The Disproportionate Role of Ocean Topography on the Upwelling of Carbon in the Southern Ocean

Riley X. Brady[1], Mathew E. Maltrud[2], Phillip J. Wolfram[2], Henri F. Drake[3], and Nicole S. Lovenduski[1]

[1]Department of Atmospheric and Oceanic Sciences and Institute of Arctic and Alpine Research, University of Colorado, Boulder, CO, USA

[2]Fluid Dynamics and Solid Mechanics (T-3), Los Alamos National Laboratory, Los Alamos, NM, USA

[3]MIT-WHOI Joint Program in Oceanography/Applied Ocean Science & Engineering, Cambridge and Woods Hole, MA, USA

Contents of this file

1. Text S1 to S2
2. Figures S1 to S5

Additional Supporting Information (Files uploaded separately)

1. Caption for Movie S1

Introduction The supporting information serves to provide a more detailed description of the Eulerian model configuration and to evaluate its performance against observations. We show the Eulerian model mesh resolution via a snapshot of dissolved inorganic carbon in the Drake Passage in Figure S1 and as a function of latitude in Figure S2. In Text S1,

we describe the use of (or lack thereof) subgrid-scale parameterizations, detail the ocean biogeochemical model, and outline the initialization and spinup strategy. In Text S2, we assess the Eulerian model's fidelity at simulating horizontal transport in the Antarctic Circumpolar Current (Figure S3), mixed layer depths (Figure S4), and deep concentrations of dissolved inorganic carbon (Figure S5).

Text S1. As mentioned in the main text, we use the ocean and sea ice components of the Energy Exascale Earth System Model (E3SM) in this study (Burrows et al., 2020), the Model for Prediction Across Scales Ocean (MPAS-O) and SeaIce (Ringler et al., 2013). Due to the high resolution of the horizontal mesh (Figure S1 and S2), we resolve mesoscale eddies and thus do not parameterize the effect of baroclinic instabilities on horizontal tracer diffusion. However, we do parameterize the effect of vertical mixing on tracer distributions using the K-profile parameterization (KPP; Large, McWilliams, and Doney (1994)).

The ocean biogeochemical component is derived from the Biogeochemical Elemental Cycling (BEC) model, which contains three phytoplankton functional types (diatoms, diazotrophs, and a small calcifying phytoplankton class), a single zooplankton class, seawater carbonate chemistry, and also tracks the cycling of C, N, P, Fe, Si, and O (Moore et al., 2013). MPAS-O adds additional features to BEC, including prognostic dimethyl sulfide (DMS) production and an explicit *Phaeocystis* phytoplankton class (Wang & Moore, 2011).

Prior to initializing the biogeochemical model, we spun up the ocean and sea ice models from rest for 25 years with CORE-II interannual forcing. We then initialized the ocean

biogeochemistry using climatologies from observationally based data products. DIC and alkalinity were initialized using pre-industrial values from the Global Ocean Data Analysis Project (GLODAP; Key et al. (2004)), and nutrients were initialized using the *World Ocean Atlas* (WOA; Garcia et al. (2013)). The physical and biogeochemical models were then spun up for 33 years to reach approximate steady-state in air-sea CO_2 fluxes in the Southern Ocean (not shown). After the spinup, the global integral of air-sea CO_2 flux has a relatively small linear drift of 0.05 PgC yr^{-2}.

Text S2. Here, we provide further evaluation of the MPAS-O simulation, focusing on horizontal transport in the ACC, mixed layer depth, and deep concentrations of DIC. We first compare the barotropic stream function (BSF) in MPAS-O to a high resolution state estimate of the Southern Ocean (Mazloff et al., 2010) in Figure S3. We find general agreement between our simulation and the state estimate, with cyclonic polar gyres in the Ross and Weddell Seas, and similar magnitudes and locations for ACC streamlines (Figure S3). Next, we assess the annual mean mixed layer depth against Argo-based observations from Holte, Talley, Gilson, and Roemmich (2017) (Figure S4). Our model reproduces the spatial patterns of the observational product, with deeper mixed layers in the ACC downstream of the Kerguelan Plateau and in the Pacific sector (Figure S4). Within the ACC (south of 45°S and outside of the annual sea ice zone), we find a pattern correlation of 0.72 with the observational product and a mean absolute error (MAE) of 21 m. Note that our model does have very deep mixed layers within the sea-ice zone due to open-ocean polynyas (not shown), which has been documented in other ocean models (Zanowski et al., 2015). While this is unlikely to affect the results of our study, it could

have an impact on tracer distributions in the Southern Ocean. Lastly, we evaluate the deep-water stores of pre-industrial DIC in our model (Figure S5). We find that MPAS-O replicates the broad-scale patterns of the observations well. MPAS-O simulates enriched stores of pre-industrial DIC within the ACC (where curl-driven upwelling occurs) and depleted pre-industrial DIC concentrations equatorward of the ACC (Figure S5). This results in a pattern correlation of 0.90 within the ACC and an MAE of 14 μmol kg^{-1}. Note that the model simulates slightly lower levels of pre-industrial DIC at depth in the ACC than observations, and thus our results likely underestimate carbon upwelling along particle trajectories.

Movie S1. Lagrangian flow of dissolved inorganic carbon (DIC) in the Southern Ocean between 300 m and 2000 m for an arbitrary year of the simulation. Output is stored and visualized in two day increments, with the previous week's history drawn to outline mesoscale eddy activity. Pathlines are colored by the instantaneous DIC recorded by the particle at model runtime.

References

Burrows, S., Maltrud, M., Yang, X., Zhu, Q., Jeffery, N., Shi, X., ... others (2020). The DOE E3SM v1. 1 biogeochemistry configuration: description and simulated ecosystem-climate responses to historical changes in forcing. *Journal of Advances in Modeling Earth Systems*, e2019MS001766.

Garcia, H. E., Locarnini, R. A., Boyer, T. P., Antonov, J. I., Baranova, O. K., Zweng, M. M., ... Levitus, S. (2013). World Ocean Atlas 2013. volume 4, dissolved inorganic nutrients (phosphate, nitrate, silicate).

Holte, J., Talley, L. D., Gilson, J., & Roemmich, D. (2017). An argo mixed layer climatology and database. *Geophysical Research Letters*, *44*(11), 5618–5626.

Key, R. M., Kozyr, A., Sabine, C. L., Lee, K., Wanninkhof, R., Bullister, J. L., ... Peng, T.-H. (2004). A global ocean carbon climatology: Results from Global Data Analysis Project (GLODAP). *Global biogeochemical cycles*, *18*(4).

Large, W. G., McWilliams, J. C., & Doney, S. C. (1994). Oceanic vertical mixing: A review and a model with a nonlocal boundary layer parameterization. *Reviews of Geophysics*, *32*(4), 363–403.

Mazloff, M. R., Heimbach, P., & Wunsch, C. (2010). An eddy-permitting Southern Ocean state estimate. *Journal of Physical Oceanography*, *40*(5), 880–899.

Moore, J. K., Lindsay, K., Doney, S. C., Long, M. C., & Misumi, K. (2013). Marine ecosystem dynamics and biogeochemical cycling in the Community Earth System Model [CESM1 (BGC)]: Comparison of the 1990s with the 2090s under the RCP4.5 and RCP8.5 scenarios. *Journal of Climate*, *26*(23), 9291–9312.

Ringler, T., Petersen, M., Higdon, R. L., Jacobsen, D., Jones, P. W., & Maltrud, M. (2013). A multi-resolution approach to global ocean modeling. *Ocean Modelling*, *69*, 211–232.

Wang, S., & Moore, J. K. (2011). Incorporating Phaeocystis into a Southern Ocean ecosystem model. *Journal of Geophysical Research: Oceans*, *116*(C1).

Zanowski, H., Hallberg, R., & Sarmiento, J. L. (2015). Abyssal ocean warming and salinification after Weddell polynyas in the GFDL CM2G coupled climate model. *Journal of Physical Oceanography*, *45*(11), 2755–2772.

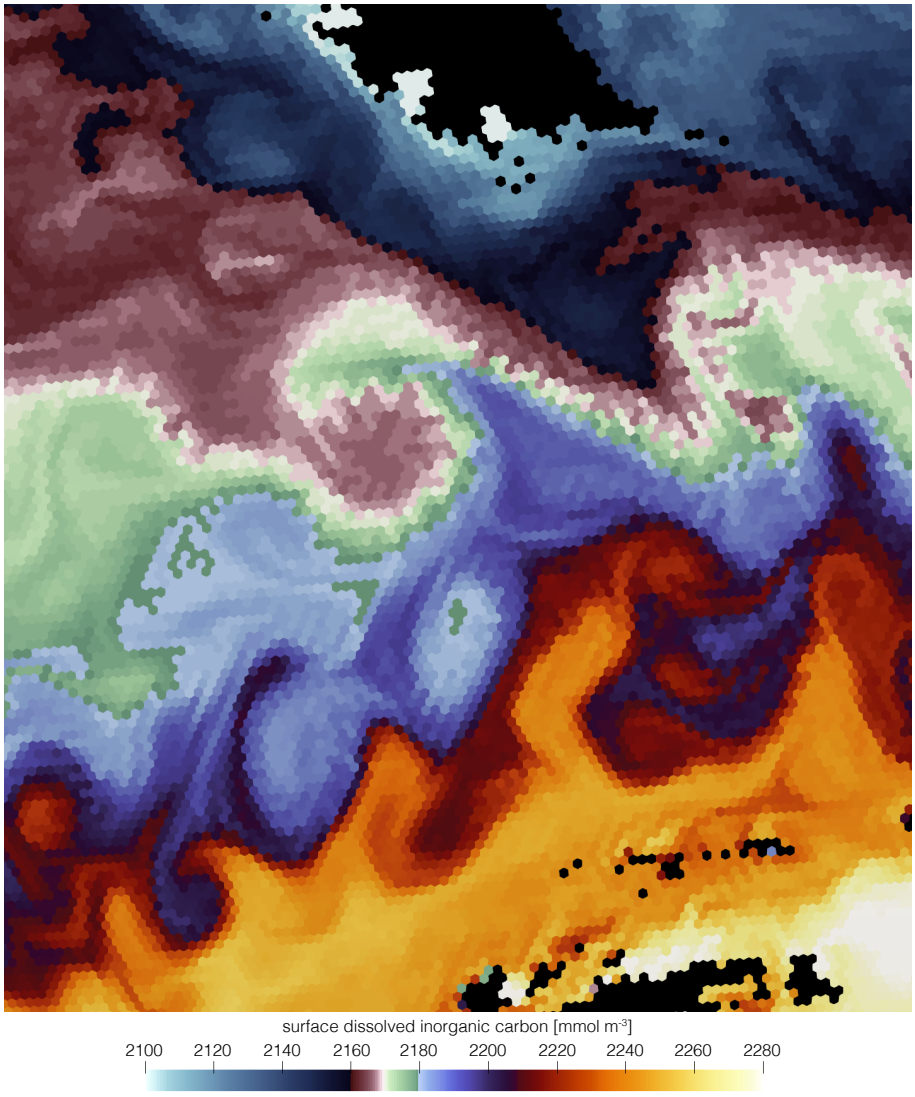

Figure S1. A snapshot of an arbitrary five-day average surface dissolved inorganic carbon (DIC) field in December. This showcases DIC levels in the Drake Passage, where black grid cells outline the southern tip of South America (top) and northern extent of the Antarctic Peninsula (bottom). Hexagonal pixels show the actual Eulerian mesh and its horizontal resolution, which is approximately 14.5 km in this region (Figure S2).

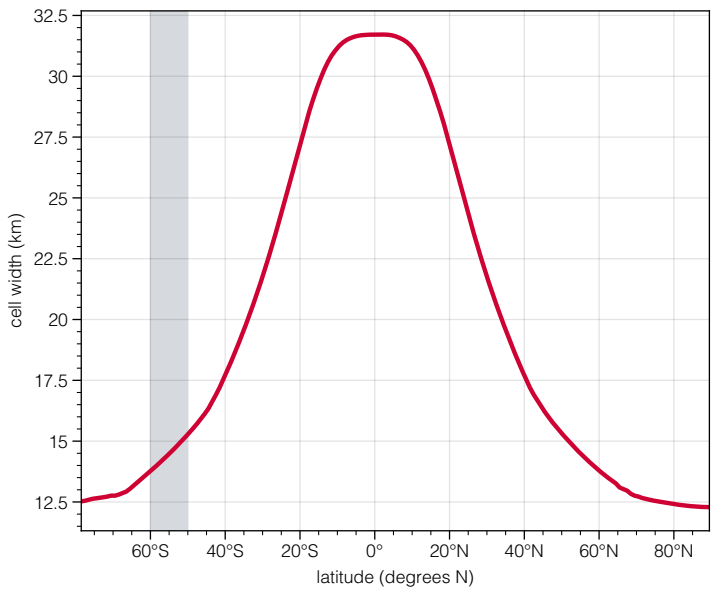

Figure S2. Horizontal resolution of grid cells for the ocean model used in this study. The average hexagonal width of the Model for Prediction Across Scales-Ocean (MPAS-O) are shown as a function of latitude, with the approximate extent of the Antarctic Circumpolar Current (50^oS–60^oS shaded in gray).

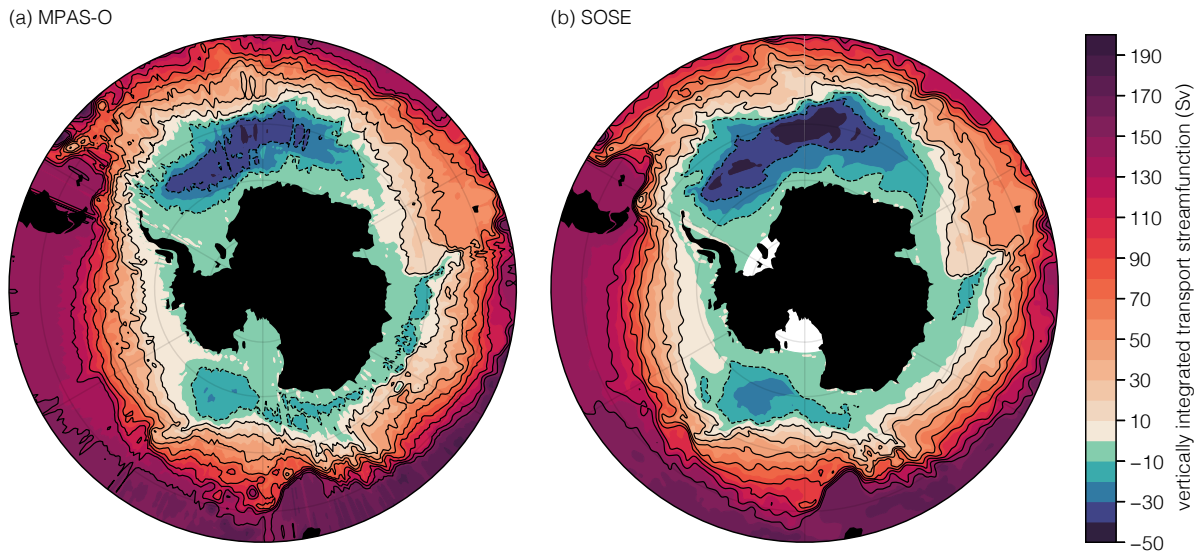

Figure S3. Model evaluation of the vertically integrated horizontal transport streamfunction. (a) Annual climatology of the barotropic streamfunction for the Model for Prediction Across Scales–Ocean (MPAS-O), the model used in this study. (b) Barotropic streamfunction for a solution of the Southern Ocean State Estimate (SOSE; Mazloff et al. (2010)). Contours outline 20 Sv increments. The model's climatology for 75% annual sea ice extent is outlined in black and mixed layer depths are not compared within this region to focus on the Antarctic Circumpolar Current.

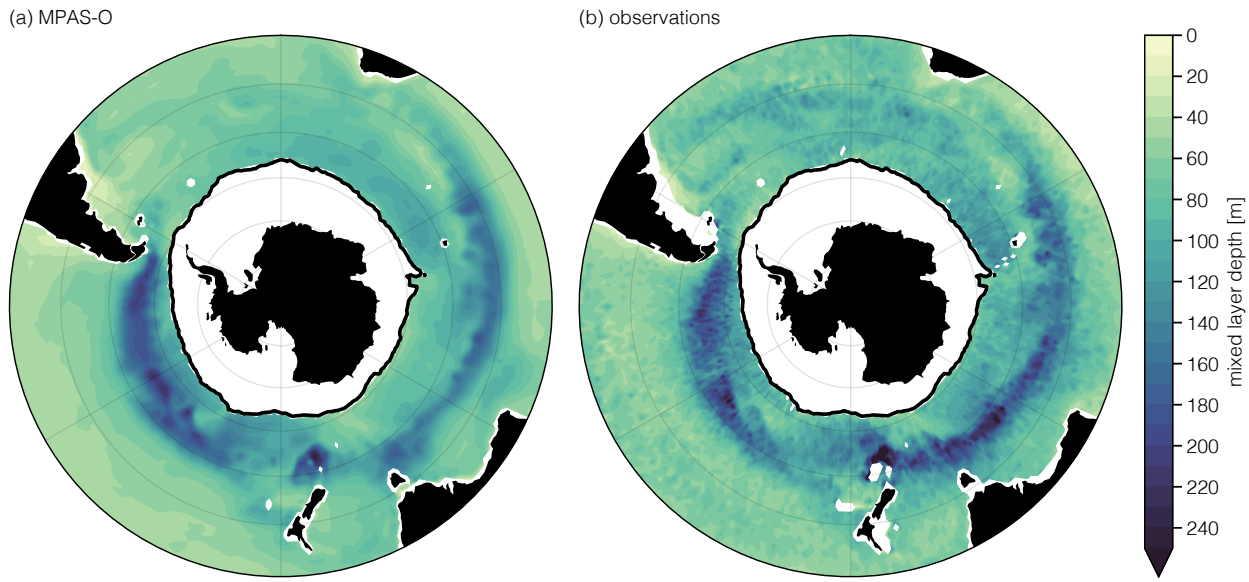

Figure S4. Model evaluation of annual mixed layer depth. (a) Annual climatology for mixed layer depth for the Model for Prediction Across Scales–Ocean (MPAS-O), the model used in this study. (b) Annual mean mixed layer depth from Holte et al. (2017)'s ARGO-based observational climatology. The model's climatology for 75% annual sea ice extent is outlined in black and mixed layer depths are not compared within this region to focus on the Antarctic Circumpolar Current.

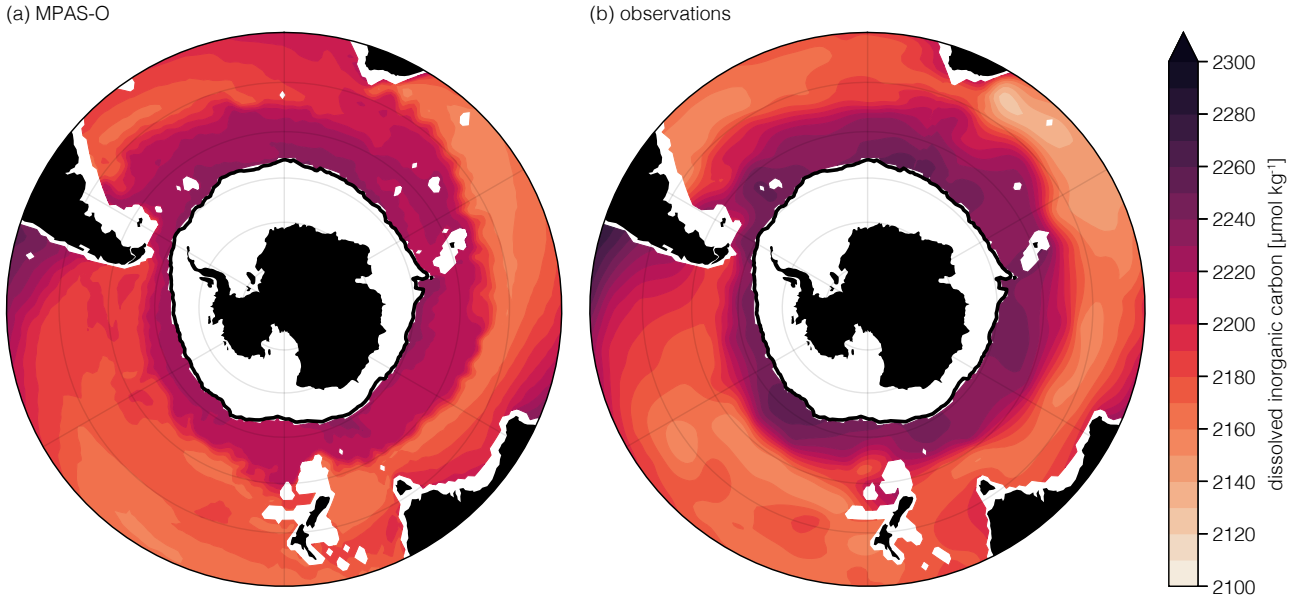

Figure S5. Model evaluation of dissolved inorganic carbon (DIC) at 1000 m. (a) Annual climatology for DIC at 1000 m for the Model for Prediction Across Scales–Ocean (MPAS-O), the model used in this study. (b) Annual mean pre-industrial DIC from the Global Ocean Data Analysis Project (GLODAP; Key et al. (2004)). The model was compared to the pre-industrial DIC observational product, since that is what was used to initialize the simulation. The model's climatology for 75% annual sea ice extent is outlined in black.